

# Multivalued Stability Map of an Injection-Locked Semiconductor Laser

Marko M. Krstić, Jasna V. Crnjanski, Milan L. Mašanović, *Member, IEEE*, Leif A. Johansson, *Member, IEEE*, Larry A. Coldren, *Fellow, IEEE*, and Dejan M. Gvozdić

**Abstract**—We present a novel and detailed analysis of the locking range and the stability map for side-mode injection-locked in-plane semiconductor multimode lasers. By including the usually neglected unlocked modes in our model, we predict a multivalued locking range and stability map for this type of lasers. We also explain and relate, the previously noticed slave laser bistability phenomenon with the multivalued character of the locking range and stability map, and experimentally validate our findings. Moreover, we find that the unstable operating region, commonly found in literature by stability analysis of the injection-locked mode alone, is actually much smaller.

**Index Terms**—Bistability, locking range, multimode semiconductor lasers, multivalued functions, stability map.

## I. INTRODUCTION

INJECTION locking is a general phenomenon observed in many disciplines such as physics, engineering, biology, etc. For the first time, it was observed by C. Huygens, who noticed that the pendulums of two clocks on the wall move in unison if the clocks are hanged close to each other [1]. Later, other examples of this phenomenon were observed, such as human circadian rhythm locking to the length of day [1], or the locking of the Moon's to the Earth's rotation. Over time, injection locking has been used in a number of engineering applications comprising oscillators: electrical [2], microwave [3], or optical, i.e., lasers [4]. Semiconductor lasers are a type of electrically driven oscillators in which the number of supported oscillations or modes can be controlled by various feedback mechanisms, providing single- or multimode operation. For a multimode laser, a sophisticated method to control oscillations in this (slave) laser relies on synchronization with another (master) laser, i.e., on the technique of injection locking.

The stable locking regime of an injection-locked laser is usually characterized by a stability map, which is represented by a set of ordered pairs comprising angular frequency of detuning

$\Delta\omega$  between the master and the slave laser free-running frequencies, and the injection power ratio  $r$  (i.e., the ratio of the photon density  $S_{inj}$  injected into the slave laser and the photon density  $S_m$  of the injection-locked mode of the slave laser) for which the slave laser is stably locked to the master laser. Such map has previously been thought to be a single-valued function on  $\Delta\omega$  and  $r$  [5]–[8]. However, in this paper, we show that the slave laser behavior is far more complex and that the stability map is a multivalued function. We arrive at this important conclusion, which revises the current understanding of the locking and the stability map, by studying, theoretically and experimentally, the effects of a side-mode injection into a Fabry–Perot in-plane quantum well laser.

In the prior work on the analysis of the stability maps [6], [7], the unlocked slave laser modes have not been taken into account, although it has been suggested that the unlocked modes should be included into the consideration in the case of their collateral excitation or gain suppression effects during the injection locking [5], [8]. Even in the case of unstable injection locking, followed by a variety of peculiar and chaotic effects, researchers were still focused only on the injection-locked mode [4], [9]. Here, we show that unlocked modes significantly impact the locking range, as well as the boundaries of the stable locking in the regions where the stability map is a single-valued function. As a consequence of the multivalued character of the stability map, we show that the bistability of the slave laser occurs within the region which was previously considered stable [5], [6]. Although the bistability was previously noticed [7], [8], it was never fully explored and explained. In this study, we also experimentally confirm and correlate this bistability with our modeling results.

In Section II, we present the model of the multimode rate equations (MREs) used in our work. In Section III, we show the locking map and theoretically explain its multivalued character. Section IV relates mapping of stationary points from  $\Delta\omega - r$  space with phase plots and provides analysis of the stability plots. In Section V, we present the experiment and its results, which we compare with our theoretical findings. Finally, in Section VI, we provide the conclusion of this paper.

## II. MODEL

The dynamics of the injection-locked slave laser is described by a system of MREs [10] with extra terms describing the locking phenomenon [4]–[10]. We consider a Fabry–Perot slave laser whose emission in the free-running regime is centered at the photon energy  $\hbar\omega_0 = 0.8$  eV ( $\lambda_0 = 1.55$   $\mu\text{m}$ ). The material gain spectrum used in the model  $g(n, \omega)$  where  $n$  stands for

Manuscript received October 31, 2012; revised December 29, 2012; accepted January 9, 2013. This work was supported by the Serbian Ministry of Education and Science (project Photonics Components and Systems 171011).

M. M. Krstić, J. V. Crnjanski, and D. M. Gvozdić are with the School of Electrical Engineering, University of Belgrade, Belgrade 11000, Serbia (e-mail: marko.krstic@etf.rs; jafa@etf.bg.ac.rs; gvozdic@etf.bg.ac.rs).

M. M. Mašanović, L. A. Johansson, and L. A. Coldren are with Electrical and Computer Engineering Department, University of California, Santa Barbara, CA 93106 USA (e-mail: mashan@ece.ucsb.edu; leif@ece.ucsb.edu; coldren@ece.ucsb.edu).

Color versions of one or more of the figures in this paper are available online at <http://ieeexplore.ieee.org>.

Digital Object Identifier 10.1109/JSTQE.2013.2241026

the carrier density and  $\omega$  for the angular photon frequency, is asymmetric. It reaches its maximum ( $g_{\text{th}} = 1222 \text{ cm}^{-1}$ ) at the threshold carrier concentration  $n = n_{\text{th}} = 2.85 \times 10^{18} \text{ cm}^{-3}$  and at the angular frequency  $\omega = \omega_0$ , corresponding to the central (dominant) mode. Due to the gain asymmetry with respect to  $\omega$ , the number of side modes which can be supported by the laser cavity is  $l_1 = 170$  for  $\omega < \omega_0$  and  $l_2 = 120$  for  $\omega > \omega_0$ .

The MREs describe the photon density for each mode in the mode ensemble. Since the phase and the photon density equations of the injection-locked side-mode are coupled with the photon density and the phase of injected light, it is necessary to add separate photon density and the phase equation of the injection-locked mode to the MRE system. Thus, the system comprises  $l_1 + l_2 + 3$  nonlinear differential equations. One of the equations deals with the carrier concentration ( $n$ ) dynamics,  $l_1 + l_2 + 1$  equations describe the time dependence of the photon density of both the injection-locked  $m$ th mode ( $S_m$ ) and other longitudinal modes ( $S_j$ ), including the central mode ( $j = 0$ ), while the last equation describes the time evolution of the phase difference  $\theta_m$  between the free-running and the injection-locked state [10]:

$$\frac{dn}{dt} = \frac{I}{qV} - [A_{\text{SRH}}n + R_{\text{sp}}(n) + C_A n^3] - \sum_{j=-l_1}^{l_2} v_g g(n, \omega_j) S_j \quad (1)$$

$$\frac{dS_j}{dt} = \Gamma v_g g(n, \omega_j) S_j - \frac{S_j}{\tau_p} + \Gamma \beta_{\text{sp}} R_{\text{sp}}(n), \quad j \neq m \quad (2)$$

$$\frac{dS_m}{dt} = \Gamma v_g g(n, \omega_m + \Delta\omega) S_m - \frac{S_m}{\tau_p} + \Gamma \beta_{\text{sp}} R_{\text{sp}}(n) + 2k_c \sqrt{S_m S_{\text{inj}}} \cos \theta_m \quad (3)$$

$$\frac{d\theta_m}{dt} = \frac{\alpha}{2} \left[ \Gamma v_g g(n, \omega_m + \Delta\omega) - \frac{1}{\tau_p} \right] - \Delta\omega - k_c \sqrt{\frac{S_{\text{inj}}}{S_m}} \sin \theta_m. \quad (4)$$

In (1),  $I = 1.2I_{\text{th}}$  is the current of the slave laser ( $I_{\text{th}} = 2.45 \text{ mA}$ ),  $R_{\text{sp}}(n)$  is the total spontaneous optical emission rate,  $A_{\text{SRH}} = 1.1 \times 10^8 \text{ s}^{-1}$  is the Shockley–Reed–Hall, and  $C_A = 5.82 \times 10^{-29} \text{ cm}^6 \text{ s}^{-1}$  is the Auger recombination constant, while  $V = 7.83 \times 10^{-12} \text{ cm}^3$  is the volume of the active area, corresponding to a laser width  $w = 1.2 \text{ }\mu\text{m}$  and the laser cavity length  $L = 250 \text{ }\mu\text{m}$ . In the system of MREs  $\tau_p = (\Gamma \cdot v_g \cdot g_{\text{th}})^{-1} = 2.04 \text{ ps}$  stands for the photon lifetime,  $\Gamma = 0.056$  is the confinement factor,  $v_g = c/n_g$  is the group velocity with  $n_g = 4.2$ ,  $k_c = 1.13 \times 10^{11} \text{ s}^{-1}$  is the external light coupling factor,  $\alpha = 3$  is the linewidth enhancement factor,  $\Delta\omega$  is the frequency detuning between the master and slave lasers, while  $\beta_{\text{sp}} = 2.15 \times 10^{-4}$  is the spontaneous emission coupling factor, defined as the ratio of spontaneous emission coupling rate to the lasing mode and total spontaneous emission rate. Finally,  $S_{\text{inj}}$  is the injected photon density, which is proportional to the injected optical power  $P_{\text{inj}}$  and is given by relation  $S_{\text{inj}} = \tau_p \cdot \Gamma \cdot P_{\text{inj}} / (\eta_0 \cdot \hbar\omega \cdot V)$ , where  $\eta_0 = 0.33$  is the optical efficiency. All numerical values for

these quantities in our model are taken from [10]. The angular frequencies of side longitudinal mode  $j$  and injection-locked mode  $m$  are denoted by  $\omega_j$  and  $\omega_m$ , respectively. We define  $\omega_j$  as the longitudinal mode frequency, separated from the dominant mode  $\omega_0$  by integer multiple  $j$  of intermodal spacing, i.e.,  $\omega_j = \omega_0 + j(\pi c/n_g L)$ , which for the injection-locked mode order  $j = m$  yields  $\omega_m = \omega_0 + m(\pi c/n_g L)$ . As already defined, the frequency of the dominant mode  $\omega_0$  is the lasing frequency in the free-running regime, corresponding to the modal gain maximum, at  $n = n_{\text{th}}$ . Since our model does not account for the variation of the group refractive index  $n_g$  with frequency or carrier density, the frequencies of all of the modes are fixed with respect to the carrier density variation in the laser and the dominant mode  $\omega_0$ . An implicit frequency variation with carrier density change for the injection-locked mode is taken into account only by (7). However, the frequency detuning  $\Delta\omega$  between the master and slave laser is defined with respect to the injection locked mode frequency  $\omega_m$ , which is the closest to the frequency of injected signal from the master laser. In our computation, injected optical power  $P_{\text{inj}}$  and the photon density in any of the modes are at least two orders of magnitude smaller than those necessary to trigger the mechanism of nonlinear gain suppression which is therefore neglected in our computation.

The system of MREs (1)–(4), can be rewritten in a more compact form, in which instead of the injected photon density  $S_{\text{inj}}$  we introduce  $r$ , previously defined as the injection power/slave laser power ratio:

$$\frac{dn}{dt} = \frac{I}{qV} - Q(n) - \sum_{j=-l_1}^{l_2} v_g g(n, \omega_j + \delta_{jm} \Delta\omega) S_j \quad (5)$$

$$\frac{dS_j}{dt} = A_j(n) S_j + B(n) + \delta_{jm} 2k_c \sqrt{r} S_j \cos \theta_j \quad (6)$$

$$\frac{d\theta_m}{dt} = \frac{1}{2} \alpha A_m(n) - \Delta\omega - k_c \sqrt{r} \sin \theta_m. \quad (7)$$

In addition, we define  $B(n) = \Gamma \beta_{\text{sp}} R_{\text{sp}}(n)$  as the effective spontaneous emission,  $A_j(n) = \Gamma v_g g(n, \omega_j + \delta_{jm} \Delta\omega) - \tau_p^{-1}$  as the effective rate of stimulated photon generation for mode  $j$ , and  $Q$  as the total recombination rate, representing the sum of  $R_{\text{sp}}(n)$  and nonradiative recombination rates. Equation (6) applies on all modes, injection-locked and unlocked, which is regulated by Kronecker delta  $\delta_{jm}$ .

### III. LOCKING RANGE ANALYSIS

Starting from the stationary (6) for  $j = m$  and (7), assuming that  $B(n)$  is negligible in comparison to the other terms, the stationary value for  $\theta_m$  is

$$\theta_m = \text{Arcsin} \left[ -\frac{\Delta\omega}{\sqrt{r k_c^2 (1 + \alpha^2)}} \right] - \arctan(\alpha). \quad (8)$$

The first term in the aforementioned equation is the generalized inverse sine, given by  $\varphi(-1)^z + z\pi$ , where  $\varphi = \arcsin\{-\Delta\omega/[k_c(1 + \alpha^2)^{1/2} r^{1/2}]\}$  is its principal value, while

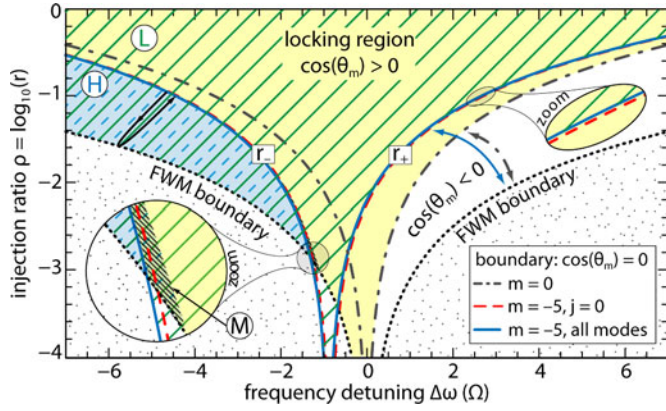


Fig. 1. Locking range for the injection into: the side mode  $m = -5$  with all unlocked modes included (single and double hatched); the central mode  $m = 0$ , excluding unlocked modes (shaded). Boundary condition  $\cos(\theta_m) = 0$  for injection into:  $m = 0$  excluding unlocked modes (dash-dot line);  $m = -5$  with the central mode ( $j = 0$ ) included (dash line);  $m = -5$  with all unlocked modes included (solid line). Distribution of the roots of (11):  $L$  (hatched),  $H$  (double-hatched),  $M$  (dense-hatched) for all modes included.

$z$  is an integer, which has a physical meaning only for  $z \in \{0, 1\}$ . By introducing  $\psi = \arctan(\alpha)$ , (8) yields

$$r = \frac{\Delta\omega^2}{k_c^2(1 + \alpha^2)\sin^2(\theta_m + \psi)} \quad (9)$$

which for real  $\theta_m$ , and extreme values for  $\sin(\theta_m + \psi) = \pm 1$  defines the boundaries between the injection-locked and the four wave mixing (FWM) regions [6]. However, an additional condition comes from the fact that in the locked range  $\cos(\theta_m) > 0$  [11]. The locking boundary can be derived from the condition  $\cos(\theta_m) = 0$ , which according to (8) can be converted to  $\sin(\theta_m) = -1$  for  $\Delta\omega > 0$  and to  $\sin(\theta_m) = +1$  for  $\Delta\omega < 0$ . Insertion of  $\sin(\theta_m) = \pm 1$  into the stationary form of (7) leads to  $\alpha A_m(n)/2 = \Delta\omega - \text{sgn}(\Delta\omega)k_c r^{1/2}$ . If the injection-locked mode is the central mode ( $m = 0$ ) at  $n = n_{\text{th}}$ , then  $A_m(n) = 0$ . In this case, the locking boundary is given by  $\Delta\omega = \pm k_c r^{1/2}$  or  $r = (\Delta\omega/k_c)^2$  (dash-dot line in Fig. 1), where  $\Delta\omega$  is given in units of  $\Omega$  ( $\Omega = 10^{10}$  rad/s). This can also be derived from (9), by taking into account that for  $\theta_m = \pm\pi/2$ ,  $\sin(\pm\pi/2 + \psi) = \pm(1 + \alpha^2)^{-1/2}$ . If  $m$  is a side mode ( $m \neq 0$ ), the stationary photon densities corresponding to  $\cos(\theta_m) = 0$  are given by  $S_j = -B(n)/A_j(n)$  for all modes. Thus, (5) can be written with respect to  $n$  as

$$\frac{I}{qV} - Q(n) + \sum_{-l_1 \leq j \leq l_2} v_j g(n, \omega_j + \delta_{jm} \Delta\omega) \frac{B(n)}{A_j(n)} = 0. \quad (10)$$

The solution to (10) in this case is  $n_c < n_{\text{th}}$ . It represents the stationary state of the laser, for which  $A_m(n_c) < 0$ . This last condition remains valid whether besides the central mode, we take into account all other side modes, a few side modes (including injection-locked mode) or only injection-locked mode  $m \neq 0$ . Therefore, the new locking boundaries (see Fig. 1) can be found from  $\alpha A_m(n_c)/2 = \pm(|\Delta\omega| - k_c r^{1/2})$ , leading to  $r_{\pm} = \{[\pm|\Delta\omega| - \alpha A_m(n_c)/2]/k_c\}^2$  where (+) corresponds to positive and small negative  $\Delta\omega$  ( $r_+$  boundary), while (-) is used

for sufficiently large negative  $\Delta\omega$  ( $r_-$  boundary). However, for the  $r_+$  boundary, this condition imposes an additional, more rigid constraint, which due to the negative value of  $A_m(n_c)$ , additionally rises the boundary of  $r$ , leading to a shrinkage of the locking range (cf., Fig. 1). In this case,  $\theta_m \in (-\pi/2, -\psi]$ , since the other branch of  $\varphi$  in (4) i.e.,  $\pi - \varphi$  leads to  $\cos(\theta_m) < 0$  and cannot be included in consideration. However, for the  $r_-$  boundary, it is possible to include both branches of  $\varphi$  (i.e.,  $\varphi$  and  $\pi - \varphi$ ), since for both of them  $\cos(\theta_m)$  can be positive. In this case,  $\theta_m \in \{[-\psi, 0] \cup (0, \pi/2)\}$  comprises  $\theta_m = \pi/2 - \psi$ , corresponding to the FWM boundary due to the fact that  $\sin(\theta_m + \psi) = 1$ . This means that for  $\Delta\omega < 0$ , FWM boundary divides  $\theta_m$  range in two segments,  $\theta_m \in [-\psi, \pi/2 - \psi]$  and  $\theta_m \in [\pi/2 - \psi, \pi/2]$ . Since FWM boundary corresponds to the smallest  $r$  for a given  $\Delta\omega$ , it can be concluded that the locking range in the  $\Delta\omega - r$  space is folded down along the FWM boundary, leading to the overlap of the two locking regions in the  $r$ -range between the FWM boundary and  $r_-$  (dash and solid line hatched region in Fig. 1). For small negative detuning ( $\Delta\omega \approx -1.13 \Omega$ ), the left FWM boundary crosses the locking range [ $\cos(\theta_m) \geq 0$ ]. The intersection of the FWM and the  $\cos(\theta_m) = 0$  boundary is possible, since at this point and its vicinity, there is more than one stationary solution, which can satisfy either one or the other condition imposed by these two boundaries. Within the locking range, the FWM boundary sets  $\theta_m$  to  $\pi/2 - \psi$ , but it becomes irrelevant, since on its both sides, injection locking is possible. The folding down along FWM boundary and overlap of the locking regions between FWM and corresponding  $r$  boundaries is also valid for  $m = 0$ . Since we are more interested in the injection-locking into side modes, we do not show this case in Fig. 1.

The locking range shown in Fig. 1, which accounts for the unlocked modes, exhibits a nonzero detuning offset for small injection ratios  $r$ . The essential reason for this is in our definition of  $\omega_m$ , and the uneven increase of the frequencies for the dominant mode and side longitudinal modes when the carrier density increases. The dominant frequency  $\omega_0$  is the lasing frequency corresponding to  $n = n_{\text{th}}$ , while  $\omega_m$  is the frequency for the injection-locked side-mode, defined in the free-running regime by  $\omega_m = \omega_0 + m(\pi c/n_g L)$ . This definition for  $\omega_m$  overestimates its value for  $n \leq n_{\text{th}}$ , since the gain change due to the carrier density change is smaller for the side mode  $m$  than for the dominant mode 0. Assuming a constant linewidth enhancement factor for both modes, a smaller gain change of the side mode leads to its smaller frequency change. Thus, the frequency maximum of a side mode  $m$ , which occurs at  $n = n_{\text{th}}$ , is smaller than the one predicted by  $\omega_m = \omega_0 + m(\pi c/n_g L)$ , which accounts for the dominant mode frequency increase. The correction term for the injection-locked mode frequency  $\omega_m$ , i.e., the frequency shift of the side-mode frequency  $\omega_m$ , is proportional to its gain defect. For example, the gain defect is zero ( $A_m = 0$ ) for the dominant mode  $m = 0$  ( $\omega_0$ ), and it is negative ( $A_m < 0$ ) for any side mode  $m \neq 0$  ( $\omega_m$ ). Therefore, side modes should exhibit a negative frequency shift (red shift) with respect to the frequencies given by  $\omega_m = \omega_0 + m(\pi c/n_g L)$ . This shift is taken into account by the first term in (7), and for small or negligible injection ratio  $r$  ( $r \approx 0$ ), in the stationary state ( $d\theta_m/dt = 0$ ), it

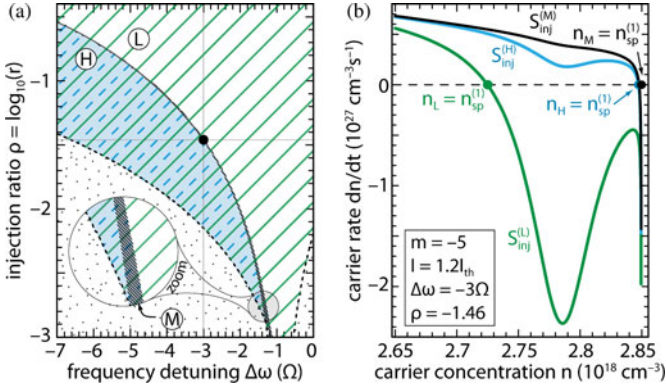


Fig. 2. (a) Distribution of roots of (11):  $L$  (hatched),  $H$  (shaded double-hatched),  $M$  (dark-dense-shaded) for all unlocked modes included. The dot corresponds to  $\Delta\omega - r$  pair, for which all three roots occur simultaneously. (b)  $dn/dt - n$  plots for all three roots and their corresponding stationary point  $n_{sp}^{(1)}$  for  $S_{inj}^{(L)} > S_{inj}^{(H)} > S_{inj}^{(M)}$ .

can be compensated only by the negative detuning offset  $\Delta\omega$ , as noticed in Fig. 1.

#### IV. STABILITY MAP ANALYSIS

From the stationary (6) for  $j = m$  and (7), one can eliminate  $\cos(\theta_m)$  and  $\sin(\theta_m)$  and derive an equation with respect to the carrier concentration  $n$ :

$$[\alpha A_m(n) - 2\Delta\omega]^2 + [A_m(n) + B(n)/S_m]^2 - 4k_c^2 r = 0. \quad (11)$$

$S_m$  can be expressed as a function of  $n$ , using the stationary form of (5) as

$$S_m = \frac{\frac{I}{qV} - Q(n) + \sum_{-l_1 \leq j \leq l_2, j \neq m} v_j g(n, \omega_j) \frac{B(n)}{A_j(n)}}{v_j g(n, \omega_m + \Delta\omega)}. \quad (12)$$

Obviously, (11) is a nonlinear equation, solutions of which are stationary concentrations  $n_s$  dependent on  $\Delta\omega$  and  $r$ . By solving (11) numerically, we find that for any  $\Delta\omega - r$  pair in the locking range (hatched region in Fig. 1), there is at least one, basic solution, which we denote as  $n_L$ , while two additional solutions may appear for  $\Delta\omega < -1.13 \Omega$  (crossing of FWM and  $r_-$  boundary). In Fig. 1,  $L$  denotes the region where there is only one solution ( $n_L$ ),  $H$  is the region where each  $\Delta\omega - r$  point represents two solutions (second-order root), the basic solution  $n_L$  and one more denoted as  $n_H$ , while  $M$  is the narrow third-order root region, which in addition to  $n_L$  and  $n_H$  comprises the third-order root region, which in addition to  $n_L$  and  $n_H$  comprises the solution  $n_M$ . In further text, by  $n_s$  we denote any of the roots  $n_L, n_H$ , or  $n_M$ . The locking boundary  $r_-$  separates the  $H$ - and  $M$ -regions (cf., Fig. 1), and with the FWM boundary outlines the  $H$ -region. For the more negative detuning ( $\Delta\omega < -2 \Omega$ ), the  $M$ -region is compressed into a line which can barely be seen.

Each  $n_s$  determines one pair of injected photon density  $S_{inj}^{(s)}$  and injection-locked mode photon density  $S_m^{(s)}$ . For a given  $S_{inj}^{(s)}$ , phase plots  $dn/dt - n$  may exhibit either one [see Fig. 2(b)] or three [see Fig. 3(b)–(d)]  $n$ -values, representing stationary points, which we denote in increasing order ( $n_{sp}^{(1)} \leq n_{sp}^{(2)} \leq$

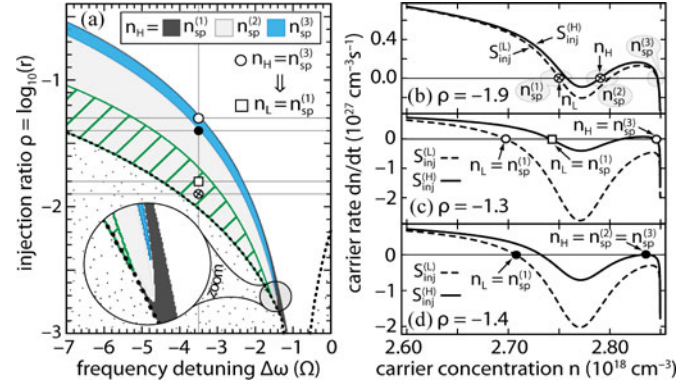


Fig. 3. (a) Partition of the  $H$ -region, with respect to the type of the stationary point  $n_H$ . The region  $n_L = n_{sp}^{(1)}$  (hatched) coexisting with  $n_H = n_{sp}^{(3)}$ . (b)  $dn/dt - n$  plot and mapping of  $n_L$  and  $n_H$  into stationary points for  $\Delta\omega = -3.5 \Omega$  and  $\rho = -1.9$ . Same for (c)  $\rho = -1.3$  and (d)  $\rho = -1.4$ . In (c)  $n_L$  for  $\rho = -1.8$  (square dot) coexists with  $n_H$  for  $\rho = -1.3$  (open dot), sharing the same injected power.

$n_{sp}^{(3)} \leq n_{th}$ ) as in [10]. Here, we analyze how the  $n_s$  roots map into these stationary points.

The root  $n_L$  from the region  $L$  corresponds to a pair  $S_{inj}^{(L)}$  and  $S_m^{(L)}$  for which there is only one stationary point in  $dn/dt - n$  phase plot, denoted as  $n_{sp}^{(1)}$ . Similarly, a point from the  $M$ -region [cf., Fig. 2(a)], maps into stationary points  $n_{sp}^{(1)}$  for each of three corresponding roots  $n_s$  [see Fig. 2(b)], all having different  $n_{sp}^{(1)}$  values, since  $S_{inj}^{(s)}$  is different for each of them.

The points from the  $H$ -region exhibit a more complex mapping. Each point from the  $H$ -region represents two roots,  $n_L$  and  $n_H$ , with two corresponding injection densities  $S_{inj}^{(L)}$  and  $S_{inj}^{(H)}$ . However, the mapping into the stationary points of the phase plot  $dn/dt - n$ , shows that  $n_L$  always maps into  $n_{sp}^{(1)}$ , while  $n_H$ , may map either into  $n_{sp}^{(2)}$  or  $n_{sp}^{(3)}$  or even into  $n_{sp}^{(1)}$  in the vicinity of the  $r_-$  boundary. Fig. 3(a) shows the full picture of the  $H$ -region partition with respect to the type of stationary point  $n_H$ . In order to provide a deeper analysis of the mapping we study character of the  $dn/dt - n$  phase plots [see Fig. 3(b)–(d)] corresponding to the  $H$ -region for a fixed detuning  $\Delta\omega = -3.5 \Omega$  and three different values of  $r$  (or  $\rho$ , where  $\rho = \log_{10} r$ ), shown by circular dots in Fig. 3(a). Fig. 3(b) shows that for  $\rho = -1.9$ ,  $n_L$  and  $n_H$  map into points  $n_{sp}^{(1)}$  and  $n_{sp}^{(2)}$ . For  $\rho = -1.3$  [see Fig. 3(c)] the situation is similar, with the exception that  $n_H$  maps into  $n_{sp}^{(3)}$ , while for the critical value  $\rho = -1.4$ ,  $n_H$  maps into a point at which  $n_{sp}^{(2)}$  and  $n_{sp}^{(3)}$  merge in the single point [see Fig. 3(d)]. As it was already mentioned, one can see from all these examples that  $n_L$  always maps into  $n_{sp}^{(1)}$ .

This analysis shows that a point from the  $H$ -region maps into two points ( $n_L$  and  $n_H$ ) each representing one stationary point in  $dn/dt - n$  phase plot [e.g., Fig. 3(b)]. Each of these points corresponds to one injected photon density  $S_{inj}^{(s)}$  and simultaneously exists with other stationary points, corresponding to the same injected photon densities,  $S_{inj}^{(L)}$  or  $S_{inj}^{(H)}$ , but different  $r$  i.e.,  $\rho$ . In these and similar cases [solid lines in Fig. 3(c) and (d)], coexistence of the stationary points may provide multistability.

Thus, we further study the range of  $r$  ( $\rho$ ), for which multi-stability may occur. We again analyze  $dn/dt - n$  plots for  $\Delta\omega = -3.5 \Omega$  and find that for  $S_{\text{inj}}^{(L)}$  and  $\rho > -1.7$ , there is only one stationary point i.e.,  $n_{\text{sp}}^{(1)}$  [dashed lines in Fig. 3(c) and (d)]. In other cases, multistability becomes feasible, since for a fixed  $S_{\text{inj}}^{(s)}$  and consequently different  $r$ -values there are three coexisting stationary points,  $n_L = n_{\text{sp}}^{(1)}$ ,  $n_H = n_{\text{sp}}^{(2)}$ , and  $n_H = n_{\text{sp}}^{(3)}$ . Fig. 3(a) shows that mapping of  $n_H$  from the  $H$ -region into  $n_{\text{sp}}^{(2)}$  or  $n_{\text{sp}}^{(3)}$ , leads to the partition of the  $H$ -region into two disjunctive subsets. However, for a fixed  $S_{\text{inj}}^{(s)}$  and detuning, each point from one subset has a corresponding point in the other [see Fig. 3(b)–(d)]. In other words, for a fixed  $S_{\text{inj}}^{(s)}$ ,  $n_{\text{sp}}^{(2)}$  and  $n_{\text{sp}}^{(3)}$  always accompany each other. Therefore, both subsets of the  $H$ -region represent ranges of multistability for stationary points  $n_{\text{sp}}^{(2)}$  and  $n_{\text{sp}}^{(3)}$ . It thus remains for us to find the multistability range corresponding to  $n_L = n_{\text{sp}}^{(1)}$ .

In order to do that, we search for the  $r$ -range for which  $n_L = n_{\text{sp}}^{(1)}$  [e.g., square dot in Fig. 3(c)] coexists with points  $n_{\text{sp}}^{(3)}$  [open dot in Fig. 3(c)] and  $n_{\text{sp}}^{(2)}$  for a fixed  $S_{\text{inj}}^{(s)}$ . For any given  $\Delta\omega$ , we find this range by calculating the photon density of the injection-locked mode  $S_m^{(L)}$  for injected density  $S_{\text{inj}}^{(L)} = S_{\text{inj}}^{(H)}$ , where  $S_{\text{inj}}^{(H)}$  corresponds to  $n_H = n_{\text{sp}}^{(3)}$  and  $n_{\text{sp}}^{(2)}$ . This finally yields  $r = S_{\text{inj}}^{(H)}/S_m^{(L)}$ . Fig. 3(a) depicts the hatched part of the  $H$ -region, in which  $n_L = n_{\text{sp}}^{(1)}$  coexists with  $n_H = n_{\text{sp}}^{(3)}$  and  $n_{\text{sp}}^{(2)}$  for the same  $S_{\text{inj}}^{(s)}$ . Moreover, in the vicinity of the  $r_-$  boundary, there is a third narrow subset in which  $n_H$  maps into  $n_{\text{sp}}^{(1)}$ , which is irrelevant for multistability.

After identifying the areas in the  $\Delta\omega - r$  space where  $n_{\text{sp}}^{(1)}$ ,  $n_{\text{sp}}^{(2)}$ , and  $n_{\text{sp}}^{(3)}$  coexist, we investigate their stability. This is done by calculating the eigenvalues of the linearized rate equations system (5)–(7), under the assumption of a small perturbation [10]. We simultaneously analyze how the number of modes included in the analysis affects the stability. For that, we investigate three cases, for which we take into account (i) the injected side-mode  $m = -5$  only, (ii) the injected side-mode  $m = -5$  and the central mode  $j = 0$ , and finally (iii) the injection-locked mode  $m = -5$  and all unlocked modes. The stationary point is considered stable if all eigenvalues of the system lie in the left-half of the complex plain, which in the cases (i)–(iii) correspond to 3, 4, and  $l_1 + l_2 + 3$  eigenvalues, respectively [6], [10]. For the case (i),  $n_L = n_{\text{sp}}^{(1)}$  corresponding to the  $L$ - and the  $H$ -region in Fig. 4(a) [shaded area, shaded area beneath the single hatched region and cross-hatched area in Fig. 4(a)] reproduces the common stability plot as predicted by earlier works [5], [6]. The union of the unlocked (blank area) and unstable region (cross-hatched area) for  $n_L = n_{\text{sp}}^{(1)}$  in Fig. 4(a) is usually classified as the region of nonlinear dynamics [6]. However, Fig. 4(a) also shows the root loci  $n_H = n_{\text{sp}}^{(2)}$ , outlining the  $H$ -region [single hatched region in Fig. 4(a)], which appear even in the single side-mode analysis. As has been explained previously, the stationary points  $n_H = n_{\text{sp}}^{(2)}$  represent an additional layer on the top of  $n_L = n_{\text{sp}}^{(1)}$  root loci in the  $H$ -region. A closer inspection shows that  $n_H = n_{\text{sp}}^{(2)}$  root behave as the

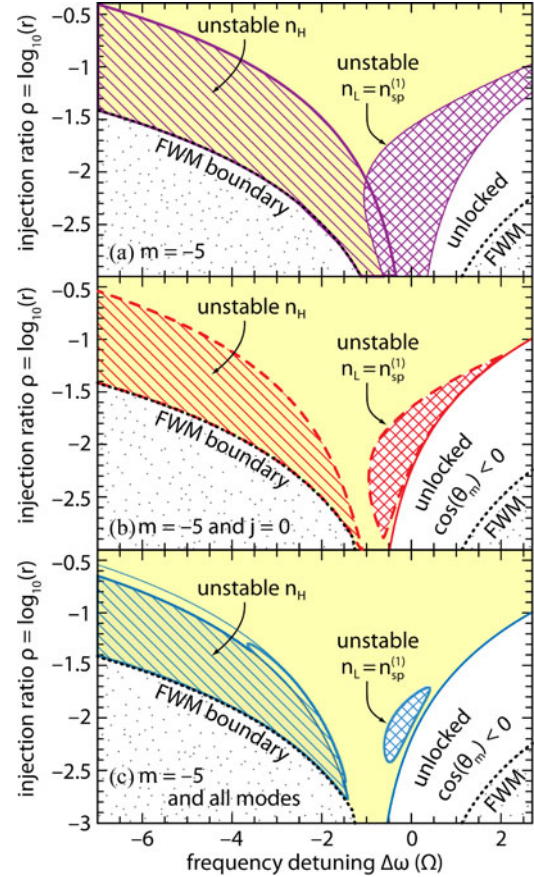


Fig. 4. (a) Stability plot for injection-locked mode  $m = -5$  alone. Stable (shaded) and unstable (hatched) part of the locking range. The whole  $H$ -region is unstable. (b) Same, for two modes included i.e., injection-locked mode  $m = -5$  and  $j = 0$ . The whole  $H$ -region is unstable. (c) Same, for all modes included. The whole subset  $n_H = n_{\text{sp}}^{(2)}$  is unstable, while  $n_H = n_{\text{sp}}^{(3)}$  is unstable only for small negative detuning. For all three cases,  $n_L$  is stable in the whole  $H$ -region (shaded under hatched).

repelling fixed point, not attracting one, as should be in case of a stable stationary point. The same is confirmed by the small signal analysis. Since the region for  $n_H = n_{\text{sp}}^{(2)}$  is fully unstable and represents the layer which overlaps  $n_L = n_{\text{sp}}^{(1)}$  layer in the  $H$ -region, one can conclude that the  $n_H$  region actually does not manifest its presence nor intersect the  $n_L = n_{\text{sp}}^{(1)}$  layer. Therefore, this single hatched layer can be ignored in case (i), while the stability map remains as the one predicted in [5], [6]. Although the  $H$ -region in case (ii) besides  $n_H = n_{\text{sp}}^{(2)}$ , comprises  $n_H = n_{\text{sp}}^{(3)}$ , we find that similarly as in case (i),  $n_H$  is fully unstable for the whole  $H$ -region [cf., Fig. 4(a) and (b)]. However, it is found in case (iii) that  $n_H = n_{\text{sp}}^{(2)}$  is always unstable, while  $n_H = n_{\text{sp}}^{(3)}$  is unstable only for a small negative detuning [see Fig. 4(c)]. For all three cases,  $n_L$  corresponding to the  $H$ -region stays stable (shaded beneath the hatched region). It can be seen in Fig. 4(b) and (c) that the unstable region for  $n_L = n_{\text{sp}}^{(1)}$  from Fig. 4(a), diminishes as the number of modes increases.

In addition to the repelling fixed point instability related to the stationary point  $n_H = n_{\text{sp}}^{(2)}$ , which can be also confirmed by

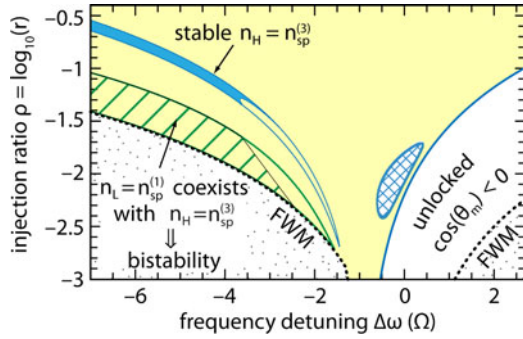


Fig. 5. Stable region for  $n_H = n_{sp}^{(3)}$  (dark shaded) and the part of  $n_L = n_{sp}^{(1)}$  (hatched) coexisting with it, for a fixed injection photon density  $S_{inj}$ , providing bistability. All modes are included.

the asymptotic Lyapunov stability check based on the small signal analysis, we find that a different type of instability is related to the other stationary points. In fact, instabilities which occur for positive detuning for  $n_L = n_{sp}^{(1)}$  and negative detuning for  $n_H = n_{sp}^{(3)}$  are related to the supercritical Hopf bifurcation, for which the laser operates on only one mode with the oscillatory output, while the suppressed modes follow the same oscillatory behavior. In the stable regions and for the fixed conditions, the slave laser remains in one of the stable points and in the injected mode over the entire range. However, the multivalued character of the locking range allows coexistence of the two stable, attractive fixed points for a sufficiently large negative detuning. As we show next, these stable points may provide shifting between modes as a result of injection power (or detuning) variation.

Since  $n_H = n_{sp}^{(3)}$  is a stable state for a sufficiently large negative detuning (see Fig. 5), we conclude that this part of locking and stability plot diagram comprises two stable solutions  $n_L$  and  $n_H = n_{sp}^{(3)}$  and represents multivalued function in  $\Delta\omega - r$  space. In addition, for fixed injected densities  $S_{inj}^{(s)}$ , the state  $n_H = n_{sp}^{(3)}$  coexists with  $n_L = n_{sp}^{(1)}$  (hatched part in Fig. 5). Therefore, we conclude that the bistability becomes feasible as a result of the multivalued character of the locking and stability plot. This result confirms that inclusion of unlocked modes in the analysis of the stability map is crucial for multimode in-plane lasers. It is not clear, whether this effect is relevant for monomode in-plane lasers. However, it can be expected that in the case of the sufficient suppression of side modes, monomode lasers can be treated as before, i.e., regardless the influence of the unlocked modes. Recent investigation of nanostructure lasers based on quantum dashes [4], [12], suggests that our findings may help to understand some of bistability effects found there. Moreover, this complete model can be useful in the investigation of the bandwidth and the modulation response of injection-locked multimode lasers [13], [14] and their dynamics in general. In addition, it can be used to study the injection-locked lasers in all-optical flip-flop element applications, to investigate the switching time between the bistable states more precisely, previously analyzed only by a single-mode model [15]. Our model can also be of interest if the injection locking includes more than one master signal, as in the case of dual injection [16].

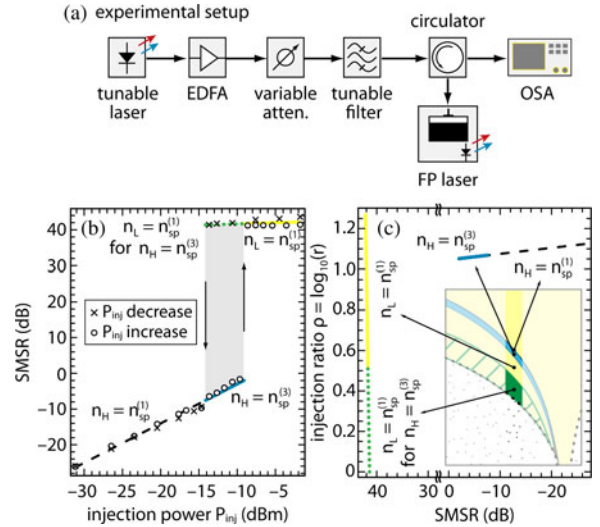


Fig. 6. (a) Experimental setup. (b) Measured SMSR for the mode  $m = -5$  versus injection power  $P_{inj}$ . (c) Branches of the hysteresis from (b), mapped into  $r$ -SMSR space: (left) upper branch within (dots) and outside (solid) bistability range; (right) lower branch within (solid) and outside (dash) bistability range. (Inset) Schematic distribution of the hysteresis branches in the locking and the stability plot.

## V. EXPERIMENT

In order to validate our findings regarding bistability, we conduct an experiment [see Fig. 6(a)], in which for a slave Fabry–Perot laser we measure the side-mode-suppression-ratio (SMSR) of the injection-locked mode  $m = -5$  (with respect to the dominant mode) versus the injection power  $P_{inj}$  [see Fig. 6(b)]. We set  $\Delta\omega = -5 \Omega$  and  $I = 1.4I_{th}$ . The decrease and then the increase of  $P_{inj}$  clearly show a hysteresis, which proves the existence of the bistability. By using the measured power corresponding to  $S_m$  for  $m = -5$  and  $P_{inj}$ , we generate the  $r$  versus SMSR plot [see Fig. 6(c)]. Since the laser used in this experiment has a larger active region volume than the one used in our calculations, we qualitatively compare Fig. 6(c) with Fig. 5 for a fixed negative detuning. The upper branch of the hysteresis loop [see Fig. 6(b)] falls into a smaller  $r$ -range ( $\rho < 0.5$ ) [see Fig. 6(c)]. This corresponds to the hatched region in Fig. 5 for which  $n_L = n_{sp}^{(1)}$  coexists with  $n_H = n_{sp}^{(3)}$ , sharing the same  $P_{inj}$ . For  $\rho > 0.5$ , corresponding to the upper branch outside of the hysteresis loop, we find only one stable stationary point. This result is supported by Fig. 5, which shows a stable region between the hatched and shaded areas, corresponding to the part of the upper branch outside of the bistability range [cf., inset in Fig. 6(c)]. For a sufficiently large  $r$  ( $\rho > 1.1$ ), there is an additional stable stationary point corresponding to lower branch of the hysteresis loop and  $n_H = n_{sp}^{(3)}$  region in Fig. 5. The fact that for this range of  $r$ , we have two different values of SMSR, i.e., two different injected powers  $P_{inj}$  for one  $r$ , confirms the conclusion that the shaded region in Fig. 5 represents the multivalued function. The lower branch outside of the loop, corresponds to  $n_H = n_{sp}^{(1)}$  [see Fig. 3(a)], which as we already mentioned, is not related to the bistability region. However, the experimental results suggest that the region corresponding to

$n_H = n_{sp}^{(1)}$  comprises a somewhat wider  $r$ -range than the one predicted by our theory, which proposes almost horizontal line for  $n_H = n_{sp}^{(1)}$  part in Fig. 6(c). It is likely that small injected powers in this case may cause a measurement uncertainty and consequently the small noticed discrepancy between the theory and the experiment. It is also possible that the experimental results include not only the  $H$ -, but also the  $M$ -region, which supports multiplicity of  $n_{sp}^{(1)}$  point. Therefore, the mapping shown in Fig. 6(c) completely resembles distribution of  $r$ -values in Fig. 5 and thin region  $n_H = n_{sp}^{(1)}$  in Fig. 3(a).

## VI. CONCLUSION

We show that the inclusion of the central and other unlocked modes in an injection-locked laser considerably modifies the commonly defined locking range map, ordinarily obtained by analysis of the injection-locked side-mode alone. For sufficient negative detuning, the locking range is degenerated and folded down between the FWM and the locking range boundary where  $\cos(\theta_m) = 0$ . Moreover, for a small  $r$ , this range is shifted toward the negative detuning. The folding down of the locking range leads to a multiplicity of the stationary points and consequently to the slave laser bistability. Qualitative agreement between our theory and our experiment has been found in this study. The stability analysis shows that when all of the modes are included in the numerical analysis, the potential bistability regions are generally stable, except for small negative detuning. However, if only the dominant and injection-locked modes are included in the stability analysis, the bistability cannot be observed since the folded part of the locking region becomes fully unstable.

Additionally, for a positive detuning, the inclusion of all unlocked modes predicts shrinkage of the unstable region on the stability map. All these results considerably modify the shape and features of the common single-valued locking and stability map [5].

## REFERENCES

- [1] A. E. Siegman, *Lasers*. Mill Valley, CA, USA: University Science Books, 1986.
- [2] R. Adler, "A study of locking phenomena in oscillators," *Proc. IRE*, vol. 34, pp. 351–357, 1946.
- [3] M. J. Fice, A. Chiuchiarelli, E. Ciaramella, and A. J. Seeds, "Homodyne coherent optical receiver using an optical injection phase-lock loop," *J. Lightw. Technol.*, vol. 29, no. 8, pp. 1152–1164, 2011.
- [4] M. C. Pochet, N. A. Naderi, V. Kovanis, and L. F. Lester, "Modeling the dynamic response of an optically-injected nanostructure diode laser," *IEEE J. Quantum Electron.*, vol. 47, no. 6, pp. 827–833, Jun. 2011.
- [5] J. Ohtsubo, *Semiconductor Lasers: Stability, Instability, Chaos*. Berlin, Germany: Springer-Verlag, 2008.
- [6] A. Murakami, "Phase locking and chaos synchronization in injection-locked semiconductor lasers," *IEEE J. Quantum Electron.*, vol. 39, no. 3, pp. 438–447, Mar. 2003.
- [7] T. B. Simpson, J. M. Liu, K. F. Huang, and K. Tai, "Nonlinear dynamics induced by external optical injection in semiconductor lasers," *Quantum Semiclass. Opt.*, vol. 9, no. 5, pp. 765–784, 1997.
- [8] T. B. Simpson, "Mapping the nonlinear dynamics of a distributed feedback semiconductor laser subject to external optical injection," *Opt. Commun.*, vol. 215, pp. 135–151, 2003.
- [9] S. Wiczorek, B. Krauskopf, and D. Lenstra, "Multipulse excitability in a semiconductor laser with optical injection," *Phys. Rev. Lett.*, vol. 88, pp. 063901–063904, 2002.

- [10] M. M. Krstić, J. V. Crnjanski, and D. M. Gvozdić, "Injection power and detuning-dependent bistability in Fabry–Perot laser diodes," *IEEE J. Sel. Topics Quantum Electron.*, vol. 18, no. 2, pp. 826–833, Apr. 2012.
- [11] C. H. Henry, N. A. Olsson, and N. K. Dutta, "Locking range and stability of injection locked 1.54  $\mu\text{m}$  InGaAsp semiconductor lasers," *IEEE J. Quantum Electron.*, vol. 21, no. 8, pp. 1152–1156, Aug. 1985.
- [12] A. Hurtado, M. Nami, I. D. Henning, M. J. Adams, and L. F. Lester, "Bistability patterns and nonlinear switching with very high contrast ratio in a 1550 nm quantum dash semiconductor laser," *Appl. Phys. Lett.*, vol. 101, pp. 161117–161121, 2012.
- [13] A. G. R. Zlitni, M. M. Krstić, and D. M. Gvozdić, "Modulation response and bandwidth of injection-locked Fabry–Perot laser diodes," *Phys. Scr.*, vol. T149, pp. 014033–014037, 2012.
- [14] X. Jin and S. L. Chuang, "Bandwidth enhancement of Fabry–Perot quantum-well lasers by injection locking," *Solid State Electron.*, vol. 50, pp. 1141–1149, 2006.
- [15] D. M. Gvozdić, M. M. Krstić, and J. V. Crnjanski, "Switching time in optically bistable injection-locking semiconductor lasers," *Opt. Lett.*, vol. 36, pp. 4200–4202, 2011.
- [16] C. W. Chow, C. S. Wong, and H. K. Tsang, "All-optical NRZ to RZ format and wavelength converter by dual-wavelength injection locking," *Opt. Commun.*, vol. 209, pp. 329–334, 2002.

**Marko M. Krstić** received the Dipl. Inž. and M.S. degrees in electrical engineering from the University of Belgrade, Belgrade, Serbia, in 2007 and 2009, respectively. He is currently working toward the Ph.D. degree in electrical engineering at the University of Belgrade.

In 2009, he joined the academic staff at the School of Electrical Engineering, University of Belgrade, where he is a Teaching and Research Assistant. His research interests include modeling and simulation of semiconductor lasers and fiber optics.

**Jasna V. Crnjanski** received the Dipl. Inž. and M.S. degrees in electrical engineering from the University of Belgrade, Belgrade, Serbia, in 2002 and 2007, respectively, where she is currently working toward the Ph.D. degree.

In 2002, she joined the School of Electrical Engineering, University of Belgrade, where she is a Teaching and Research Assistant. Her research interests include modeling of optical properties of semiconductor nanostructures. She has coauthored more than ten publications.

**Milan L. Mašanović** (S'98–M'04) received the Dipl. Inž. degree from the School of Electrical Engineering, University of Belgrade, Belgrade, Serbia, and the M.S. and Ph.D. degrees from the University of California at Santa Barbara, Santa Barbara, USA in 1998, 2000, and 2004, respectively, all in electrical engineering.

He is currently an Associate Project Scientist at the University of California at Santa Barbara, and one of the principals at Freedom Photonics LLC, a photonic integration company he cofounded in Santa Barbara. His current research interests include semiconductor lasers and photonic integrated circuits. He has coauthored more than 85 research papers, has given numerous invited talks, and has coauthored one graduate-level text book.

Dr. Mašanović was the recipient of numerous awards and fellowships, including the 2004 IEEE Lasers and Electro-Optics Society Graduate Student Fellowship Award. He serves on technical program committees for a number of conferences in the area of integrated photonics.

**Leif A. Johansson** (M'04) received the Ph.D. degree in engineering from University College London, London, U.K., in 2002.

He is currently a Research Scientist with the University of California at Santa Barbara, Santa Barbara, USA, and a principal at Freedom Photonics LLC, a photonic integration company he cofounded in Santa Barbara. His current research interests include design and characterization of integrated photonic devices for analog and digital applications and analog photonic systems and subsystems. He has coauthored more than 100 papers, and presented at numerous conferences.

**Larry A. Coldren** (S'67–M'72–SM'77–F'82) received the Ph.D. degree in electrical engineering from Stanford University, Stanford, CA, USA, in 1972.

He is the Fred Kavli Professor of optoelectronics and sensors with the University of California (UCSB), Santa Barbara. After 13 years in the research area with Bell Laboratories, Holmdel, NJ, he joined UCSB in 1984, where he is currently with the Department of Materials and the Department of Electrical and Computer Engineering. In 1990, he cofounded optical concepts, later acquired as Gore Photonics, to develop novel vertical-cavity surface-emitting laser (VCSEL) technology, and in 1998, he cofounded Agility Communications, Inc., Goleta, CA, later acquired by JDS Uniphase Corporation (JDSU), Milpitas, CA, to develop widely tunable integrated transmitters. At Bell Laboratories, he was initially on waveguided surface-acoustic-wave signal processing devices and coupled-resonator filters. He later developed tunable coupled-cavity lasers using novel reactive-ion etching technology that he created for the new InP-based materials. At UCSB, he continued work on multiple-section tunable lasers, in 1988, inventing the widely tunable multielement mirror concept, which is currently used in some JDSU products. Near this time period, he also made seminal contributions to efficient VCSEL designs that continued to be implemented in practical devices till this day. More recently, his group has developed high-performance InP-based photonic integrated circuits as well as high-speed VCSELs, and they continue to advance the underlying materials growth and fabrication technologies. He has authored or co-authored over 1000 journals and conference papers, seven book chapters, and one textbook and has been issued 64 patents. He has presented dozens of invited and plenary talks at major conferences.

Prof. Coldren is a fellow of the Optical Society of America and a member of the National Academy of Engineering. He was a recipient of the John Tyndall and Aron Kressel Awards, in 2004 and 2009, respectively.

**Dejan M. Gvozdić** received the M.S. and Ph.D. degrees in electrical engineering from University of Belgrade, Belgrade, Serbia, in 1992 and 1995, respectively.

In 1989, he joined the School of Electrical Engineering, University of Belgrade, where he currently is a Professor of Physical Electronics, Quantum Electronics and Optical Communications. His general research interests are modeling and simulation of optoelectronic devices as nanostructure lasers, optical amplifiers, photodetectors and since recently spintronic effects. He has authored and co-authored over 30 peer-reviewed journal papers. He is a recipient of several scientific awards, and has been working as a referee for a number of IEEE publications and conferences.